

# Optimal Finite-time Maxwell's Demons in Langevin Systems

Takuya Kamijima,<sup>1,\*</sup> Asuka Takatsu,<sup>2,3</sup> Ken Funo,<sup>1</sup> and Takahiro Sagawa<sup>1,4</sup>

<sup>1</sup>*Department of Applied Physics, The University of Tokyo, 7-3-1 Hongo, Bunkyo-ku, Tokyo 113-8656, Japan*

<sup>2</sup>*Department of Mathematical Sciences, Tokyo Metropolitan University, 1-1 Minami-osawa, Hachioji-shi, Tokyo, Japan*

<sup>3</sup>*RIKEN Center for Advanced Intelligence Project (AIP), 1-4-1 Nihonbashi, Chuo-ku, Tokyo, Japan*

<sup>4</sup>*Quantum-Phase Electronics Center (QPEC), The University of Tokyo, 7-3-1 Hongo, Bunkyo-ku, Tokyo 113-8656, Japan*

We identify the optimal protocols to achieve the minimal entropy production in finite-time information exchange processes in Langevin systems, on the basis of optimal transport theory. Our general results hold even for non-Gaussian cases, while we derive a concise expression of the minimal entropy production for Gaussian processes. In particular, we apply our results to Maxwell's demons that perform measurement and feedback, and demonstrate Gaussian and non-Gaussian models of optimal demons operating in finite time. Our results provide a general strategy for controlling Langevin systems, including colloidal particles and biomolecules, in a thermodynamically optimal manner beyond the quasi-static limit.

**Introduction.**— The concept of Maxwell's demon dates back to the nineteenth century, with its modern formulation being developed within the framework of stochastic thermodynamics, where the demon is formulated to perform measurement and feedback on thermodynamic systems [1, 2]. The fundamental thermodynamic costs of the demon's operations, such as measurement, feedback and information erasure, have been revealed as an extension of the second law of thermodynamics incorporating information [3–10] and demonstrated experimentally [11–17]. While the optimal protocols to achieve the fundamental second-law bounds have been established [2], such protocols in general incorporate infinitely slow driving and are unattainable in finite time. Despite growing interest in finite-time thermodynamic bounds such as the thermodynamic speed limits [18–27] and the thermodynamic uncertainty relations [28–36], the finite-time thermodynamics of information [37–45] is yet to be established.

In this Letter, we address this issue by solving an optimization problem for the entropy production (EP) in finite-time information exchange processes in bipartite overdamped Langevin systems. Specifically, we consider the finite-time tradeoff relation between the EPs of two subsystems (see also Fig. 1 later), which provides the minimum EPs and the corresponding optimal protocols. In view of optimal transport theory [46, 47], the minimum EPs have a clear geometrical meaning and are expressed as Wasserstein distances. Such Wasserstein distance can be efficiently computed by utilizing monotone maps even for non-Gaussian distributions [48]. Furthermore, the minimum EPs can be expressed concisely for Gaussian cases, based solely on the correlation coefficients.

An important application of our theory is Maxwell's demon, where the subsystems play the roles of the engine and the demon's memory. In such setups, our general results lead to the optimal energy costs for measurement and feedback in finite time, as will be demonstrated by both Gaussian and non-Gaussian models of the demons. Moreover, we intro-

duce a characteristic time that determines whether Maxwell's demons can be realized within a given operation time. These results would be useful for designing various experimental systems modeled by overdamped Langevin dynamics.

**Setup.**— We consider bipartite overdamped systems, where subsystems exchange information quantified by mutual information [6, 9]. The total system is denoted as  $XY$  and the subsystems are denoted as  $X$  and  $Y$ . While these subsystems are regarded as the engine and the memory in the Maxwell's demon situations, we do not restrict our setup to such situations at this stage. The total system is described by the two-dimensional spatial coordinate  $\mathbf{r} = [x, y]^T$  with  $T$  representing transpose, and the probability distribution  $p_{XY}(\mathbf{r}, t)$  follows the Fokker-Planck equation [49]:

$$\partial_t p_{XY} = -\nabla^T (\mathbf{v} p_{XY}), \quad (1)$$

$$\mathbf{v} = -\mu(\nabla V - \mathbf{F} + T \nabla \ln p_{XY}), \quad (2)$$

where  $\nabla$  represents the gradient,  $\mathbf{v} = [v_X, v_Y]^T$  represents the mean local velocity, and  $\mu$  denotes the mobility constant. The forces acting on the system consist of the conservative force  $-\nabla V(\mathbf{r}, t)$  and the nonconservative force  $\mathbf{F}(\mathbf{r}, t)$ . The total EP of the total system and the partial EPs of the subsystems are respectively given by [50–52]

$$\sigma_{XY} = \frac{1}{\mu T} \int_0^\tau dt \int d\mathbf{r} \|\mathbf{v}(\mathbf{r}, t)\|^2 p_{XY}(\mathbf{r}, t), \quad (3)$$

$$\sigma_i = \frac{1}{\mu T} \int_0^\tau dt \int d\mathbf{r} v_i(\mathbf{r}, t)^2 p_{XY}(\mathbf{r}, t) \quad (i = X, Y). \quad (4)$$

These EPs are nonnegative in accordance with the second law and characterize energetic dissipation. Importantly, the total EP is connected to the work and the nonequilibrium free energy of the total system,  $\mathcal{F}_{XY}$ , through the expression  $\sigma_{XY} = (-W - \Delta \mathcal{F}_{XY})/T$ .

We consider the time evolution from the initial distribution  $p_{XY}^o$  to the final distribution  $p_{XY}^f$  over the finite time  $\tau$ . These

distributions and time are fixed throughout the optimizations discussed in the following. The potential  $V$  and the non-conservative force  $\mathbf{F}$  are manipulated to drive the evolution  $p_{XY}^o \rightarrow p_{XY}^f$ . It is known that the finite-time evolution involves a finite amount of energetic dissipation, which can be minimized over the driving protocols  $V(t)$ ,  $\mathbf{F}(t)$  [53, 54]:

$$\sigma_{XY}^* := \min_{\substack{\{V, \mathbf{F}\}_{0 \leq t \leq \tau} \\ \text{s.t. } p_{XY}^o \rightarrow p_{XY}^f}} \sigma_{XY} = \frac{\mathcal{W}(p_{XY}^o, p_{XY}^f)^2}{\mu T \tau}. \quad (5)$$

Here,  $\mathcal{W}(p, q)$  represents the ( $L^2$ -) Wasserstein distance between the probability distributions  $p$  and  $q$  (with finite second moments), defined as [47]

$$\mathcal{W}(p, q)^2 := \min_{\mathcal{T} \text{ s.t. } p \rightarrow q} \int d\mathbf{r} \|\mathcal{T}(\mathbf{r}) - \mathbf{r}\|^2 p(\mathbf{r}), \quad (6)$$

where  $\mathcal{T}$  denotes transport maps from  $p$  to  $q$ , that is,  $p(\mathbf{r}) = |\det(\partial \mathcal{T}(\mathbf{r}) / \partial \mathbf{r})| q(\mathcal{T}(\mathbf{r}))$  holds. The optimal protocol for achieving Eq. (5) is constructed from the optimal transport map of Eq. (6) [54, 55]. Under this protocol, the probability distribution evolves along the geodesic of the Wasserstein metric between  $p_{XY}^o$  and  $p_{XY}^f$ . The finite-time thermodynamic bound (5) has been extensively studied for both one-dimensional and Gaussian cases [38, 40, 56–59].

*Main results.*— We first overview the general structure of our optimization problem considered in this Letter. We start with the tradeoff relation between the partial EPs of subsystems  $X$  and  $Y$  in finite time. Figure 1 illustrates the tradeoff relation (the blue curve) as the boundary of the realizable values of the partial EPs ( $\sigma_X, \sigma_Y$ ) (the shaded region). We note that the blue curve is regarded as the Pareto front in the terminology of optimization problems. The optimal values of  $\sigma_X, \sigma_Y$  are denoted as  $\sigma_X^*, \sigma_Y^*$ , respectively. One can further optimize the EP of  $X$  (resp.  $Y$ ) under the condition of  $\sigma_Y = \sigma_Y^*$  (resp.  $\sigma_X = \sigma_X^*$ ), which is written as  $\sigma_X^*|_{\sigma_Y=\sigma_Y^*}$  (resp.  $\sigma_Y^*|_{\sigma_X=\sigma_X^*}$ ) as indicated by the blue (resp. orange) square in Fig. 1. In general,  $\sigma_X^*|_{\sigma_Y=\sigma_Y^*}$  is larger than  $\sigma_X^*$  as a consequence of the tradeoff relation. We note that the global optimal value of Eq. (5) corresponds to the gray square in Fig. 1.

Our first main result is a general formula that connects the minimum partial EP and the Wasserstein distance (see Supplemental Material [60] for the proof):

$$\sigma_Y^* := \min_{\substack{\{V, \mathbf{F}\}_{0 \leq t \leq \tau} \\ \text{s.t. } p_{XY}^o \rightarrow p_{XY}^f}} \sigma_Y = \frac{\mathcal{W}(p_Y^o, p_Y^f)^2}{\mu T \tau}, \quad (7)$$

where  $p_Y^{o/f}$  denote the marginal distributions of  $p_{XY}^{o/f}$  for the subsystem  $Y$ . The optimal protocol is constructed from the transport map in the form of  $\mathcal{T}(\mathbf{r}) = [\mathcal{T}_{X|Y}(x; y), \mathcal{T}_Y^*(y)]^T$ . Here, the optimal map for  $Y$ , denoted as  $\mathcal{T}_Y^*$ , implements

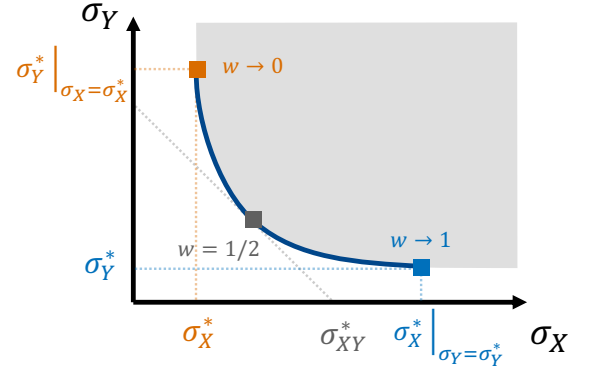


FIG. 1. Schematic of the tradeoff relation between the partial EPs in finite time. The shaded region represents realizable values of the partial EPs ( $\sigma_X, \sigma_Y$ ), whose boundary is the blue curve representing the tradeoff relation. The partial EPs are minimized at the endpoints of this curve (marked by the orange and blue squares). The blue curve is the Pareto front of conflicting quantities  $\sigma_X$  and  $\sigma_Y$  (see Supplemental Material for details). In general, such Pareto front can be obtained by minimizing  $(1-w)\sigma_X + w\sigma_Y$  with sweeping the weight  $0 < w < 1$ , where taking the limit of  $w \rightarrow 0$  and  $w \rightarrow 1$  respectively yield the orange and blue squares. The gray square ( $w = 1/2$ ) depicts the global optimal pair  $(\sigma_X, \sigma_Y)$  that achieves Eq. (5).

nothing but the one-dimensional optimal transport for  $Y$ . On the other hand,  $\mathcal{T}_{X|Y}$  is a transport map from  $p_{X|Y}^o(\cdot|y)$  to  $p_{X|Y}^f(\cdot|\mathcal{T}_Y^*(y))$ . Here,  $p_{X|Y}^o(\cdot|y)$  and  $p_{X|Y}^f(\cdot|\mathcal{T}_Y^*(y))$  represent the conditional distributions of  $X$  given the states  $y$  and  $\mathcal{T}_Y^*(y)$  of  $Y$ , respectively. In general, there are multiple such transport maps  $\mathcal{T}_{X|Y}$ , while we will discuss one of them later (Eq. (9)). In contrast,  $\mathcal{T}_Y^*$  is unique and constructed as the monotone map  $\mathcal{T}_Y^*(y) = \Gamma_Y^{f-1}(\Gamma_Y^o(y))$  [48], where  $\Gamma_Y^{o/f}(y) := \int_{-\infty}^y dy' p_Y^{o/f}(y')$  represent the cumulative distribution functions and  $\Gamma_Y^{o/f-1}(s)$  are their inverse functions. We note that it was pointed out in Ref. [40] that  $\sigma_Y$  is lower-bounded by the right-hand side of Eq. (7); we here found that the equality is indeed achievable as Eq. (7) and identified its optimal protocol.

We next consider the situation where the EP of  $X$  is minimized after minimizing the EP of  $Y$ , which corresponds to the blue square in Fig. 1. Our second main result is the minimum EP of  $X$  under the condition of minimum EP of  $Y$ , which is given by (see Supplemental Material for the proof):

$$\begin{aligned} \sigma_X^*|_{\sigma_Y=\sigma_Y^*} &:= \min_{\substack{\{V, \mathbf{F}\}_{0 \leq t \leq \tau} \text{ s.t. } p_{XY}^o \rightarrow p_{XY}^f \\ \sigma_Y=\sigma_Y^*}} \sigma_X \\ &= \frac{1}{\mu T \tau} \int dy p_Y^o(y) \mathcal{W}\left(p_{X|Y}^o(\cdot|y), p_{X|Y}^f(\cdot|\mathcal{T}_Y^*(y))\right)^2. \end{aligned} \quad (8)$$

The term  $\mathcal{W}\left(p_{X|Y}^o(\cdot|y), p_{X|Y}^f(\cdot|\mathcal{T}_Y^*(y))\right)$  represents the Wasserstein distance between the conditional distributions.

The optimal transport map is expressed as  $\mathcal{T}^{*,1}(\mathbf{r}) = [\mathcal{T}_{X|Y}^*(x; y), \mathcal{T}_Y^*(y)]^T$ , where the transport map for  $X$  is given by the following monotone map:

$$\mathcal{T}_{X|Y}^*(x; y) = \Gamma_{X|Y}^{f^{-1}} \left( \Gamma_{X|Y}^o(x; y); \mathcal{T}_Y^*(y) \right). \quad (9)$$

Here,  $\Gamma_{X|Y}^{o/f}(x; y) := \int_{-\infty}^x dx' p_{X|Y}^{o/f}(x'|y)$  denote the cumulative distribution functions of the conditional distributions and  $\Gamma_{X|Y}^{o/f-1}(s; y)$  are their inverse functions with respect to  $x$ . This transport map  $\mathcal{T}^{*,1}$  is referred to as the Knothe–Rosenblatt map in mathematics [47].

The above results also hold by exchanging  $X$  and  $Y$ . We note that  $\sigma_Y^*$  and  $\sigma_X^*|_{\sigma_Y=\sigma_Y^*}$ , as well as  $\sigma_{XY}^*$ , are inversely proportional to the time interval  $\tau$ , which is a universal characteristic of the thermodynamic speed limit [18, 20, 22].

We describe the optimal protocol  $(V^{*,1}, \mathbf{F}^{*,1})$  to achieve Eq. (8) for general distributions. Similar to the case of minimizing the total EP [54], the optimal protocol is constructed as

$$\begin{aligned} & \mu \left( -\nabla V^{*,1}(\mathbf{r}, t) + \mathbf{F}^{*,1}(\mathbf{r}, t) - T \nabla \ln p_{XY}(\mathbf{r}, t) \right) \\ &= \frac{1}{t} (\mathbf{r} - \mathbf{r}^o) \mathcal{T}^{*,1}(\mathbf{r}^o, t) = \mathbf{r}, \end{aligned} \quad (10)$$

where  $\mathbf{r}^o$  represents the initial point mapped to  $\mathbf{r}$  by the optimal Lagrange map  $\mathcal{T}^{*,1}(\mathbf{r}, t) := (1 - t/\tau)\mathbf{r} + (t/\tau)\mathcal{T}^{*,1}(\mathbf{r})$ . Thus,  $-\nabla V^{*,1}$  consists of the geodesic term  $T \nabla \ln p_{XY}(\mathbf{r}, t)$  and the gradient part of the right-hand side of Eq. (10), while  $\mathbf{F}^{*,1}$  comprises the nongradient part of the right-hand side. The right-hand side of Eq. (10) functions as the counteradiabatic term ( $\propto \tau^{-1}$ ) which drives the system along its trajectory [61]. It is worth noting that the nonconservative force is required in the optimal protocol to achieve Eq. (8) (except in the uncorrelated case), which differs from the case of Eq. (5) [53, 54]. This is because  $x^o, y^o$  in Eq. (10) become distinct gradient functions, each originating from the different maps:  $\mathcal{T}_{X|Y}^*, \mathcal{T}_Y^*$ .

*Gaussian case.*— To obtain more explicit formulas for Eqs. (7)(8), we consider special cases where the initial and final distributions are Gaussian, written as  $\mathcal{N}(\mathbf{m}^{o/f}, \Sigma^{o/f})$  with means  $\mathbf{m}^{o/f}$  and covariance matrices  $\Sigma^{o/f}$ . Let  $\rho_{o/f} := \Sigma_{XY}^{o/f} / \sqrt{\Sigma_{XX}^{o/f} \Sigma_{YY}^{o/f}}$  be the (Pearson) correlation coefficients. Then, we can analytically calculate Eq. (7) and Eq. (8), resulting in

$$\sigma_Y^* = \frac{(m_Y^o - m_Y^f)^2 + \left( \sqrt{\Sigma_{YY}^o} - \sqrt{\Sigma_{YY}^f} \right)^2}{\mu T \tau}, \quad (11)$$

$$\begin{aligned} \sigma_X^*|_{\sigma_Y=\sigma_Y^*} &= \sigma_X^* + \frac{2\sqrt{\Sigma_{XX}^o \Sigma_{XX}^f}}{\mu T \tau} \\ &\cdot \left( 1 - \rho_o \rho_f - \sqrt{(1 - \rho_o^2)(1 - \rho_f^2)} \right). \end{aligned} \quad (12)$$

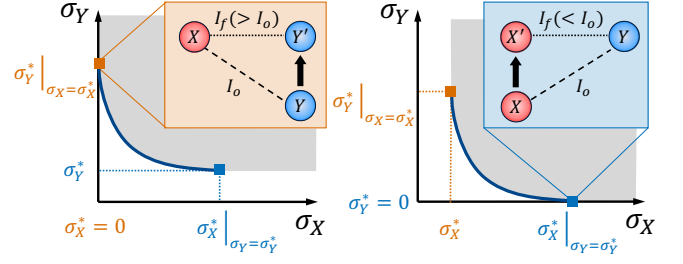


FIG. 2. Schematics for optimal measurement and feedback, which are realized at the endpoints of the Pareto front. At the orange (blue) square in the left (right) figure, the optimal measurement (feedback) is obtained by optimizing the EP of  $Y$  ( $X$ ) under the condition of  $\sigma_X^* = 0$  ( $\sigma_Y^* = 0$ ). The marginal distribution of  $X$  ( $Y$ ) is fixed in the left (right) figure, representing an ideal function of measurement (feedback).

See Supplemental Material for details. Applying the inequality  $(a + b)/2 \geq \sqrt{ab}$  for  $a, b > 0$ , Eq. (12) is lower-bounded as

$$\sigma_X^*|_{\sigma_Y=\sigma_Y^*} - \sigma_X^* \geq \frac{\sqrt{\Sigma_{XX}^o \Sigma_{XX}^f}}{\mu T \tau} (\rho_o - \rho_f)^2 \geq 0. \quad (13)$$

Both the first and second inequalities in Eq. (13) are achieved if and only if  $\rho_o = \rho_f$ . In that case, the tradeoff relation (the blue curve in Fig. 1) collapses to a single point, and thus there is a unique optimum shared by both subsystems. That is, when the correlation remains unchanged during the dynamics,  $\sigma_X$  and  $\sigma_Y$  can be simultaneously optimized.

*Application to Maxwell's demons.*— We apply our general results to Maxwell's demon setups, where  $X$  is the engine and  $Y$  is the demon's memory. These two subsystems exchange information, which is quantified by the mutual information difference. In particular, we consider measurement and feedback processes, illustrated in Fig. 2.

In the measurement process,  $X$  does not evolve but  $Y$  evolves depending on the state of  $X$ , so that they create correlation described by the mutual information difference  $\Delta I = I_f - I_o > 0$  (Fig. 2 left). During this process, the marginal distributions of  $X$  are fixed, and thus  $\sigma_X^* = 0$  holds from Eq. (7) (by exchanging  $X$  and  $Y$ ). The corresponding optimal transport map for  $X$  is given by  $\mathcal{T}_X^*(x) = x$ . The minimum energy cost for measurement is then determined through Eq. (7):

$$\frac{W - \Delta \mathcal{F}_Y}{T} - \Delta I = \sigma_Y \geq \sigma_Y^*|_{\sigma_X=\sigma_X^*}, \quad (14)$$

where  $W$  represents the work applied to  $Y$  and  $\mathcal{F}_Y$  represents its nonequilibrium free energy [2, 5]. In  $\tau \rightarrow \infty$ , Eq. (14) reduces to the bound obtained in Refs. [4, 6].

We next consider the feedback process, where  $Y$  functions as the memory, and the engine  $X$  receives feedback based on

$Y$ 's record (Fig. 2 right). To this end, we consider the initial and final distributions such that the marginal distribution for  $Y$  remains unchanged ( $p_Y^o = p_Y^f$ ) and the mutual information is consumed through the feedback, i.e.,  $\Delta I = I_f - I_o < 0$ . In this case,  $\sigma_Y^* = 0$  holds from Eq. (7) and the corresponding optimal transport of  $Y$  is given by  $\mathcal{T}_Y^*(y) = y$ . The optimal extractable work via feedback is determined through Eq. (7):

$$\frac{-W_{\text{ext}} - \Delta \mathcal{F}_X}{T} - \Delta I = \sigma_X \geq \sigma_X^*|_{\sigma_Y = \sigma_Y^*}, \quad (15)$$

where  $W_{\text{ext}}$  represents the work extracted from  $X$  and  $\mathcal{F}_X$  represents its nonequilibrium free energy. In  $\tau \rightarrow \infty$ , Eq. (14) reduces to the bound obtained in Refs. [3, 6]. We note that, while a bound of the form Eq. (15) has also been obtained in Ref. [41], the optimal protocol to achieve Eq. (15) and explicit models to realize optimal finite-time demons were unexplored in literature.

We next show that when the operation time  $\tau$  is too short for the feedback process, Maxwell's demon cannot be realized. Due to the time-dependence of  $\sigma_X^*|_{\sigma_Y = \sigma_Y^*} (\propto \tau^{-1})$ , there exists a characteristic time  $\tau_{\text{demon}} (< \infty)$  at which  $\sigma_X^*|_{\sigma_Y = \sigma_Y^*} = -\Delta I$  holds. If the feedback is implemented sufficiently slowly ( $\tau > \tau_{\text{demon}}$ ) and optimally, the extracted work  $W_{\text{ext}}$  can exceed the free energy difference  $-\Delta \mathcal{F}_X$ , thereby realizing Maxwell's demon. In contrast, Maxwell's demon cannot be realized, regardless of optimization, for fast processes satisfying  $\tau \leq \tau_{\text{demon}}$ . For non-optimal protocols,  $\tau_{\text{demon}}$  can also be defined in a similar manner. This is because the constraint  $p_{XY}^o \rightarrow p_{XY}^f$  remains satisfied by varying the operation time  $\tau$  as long as the  $t/\tau$  dependency remains the same. Since  $\tau_{\text{demon}}$  is minimized for the optimal protocol, this parameter characterizes the optimality of the given protocol. We note that the feasibility of implementing Maxwell's demon in finite time has also been studied for discrete systems in Ref. [44].

*Gaussian model of Maxwell's demon.*— We demonstrate an optimal feedback process that realizes Maxwell's demon in finite time (Eq. (15)) by a Gaussian model. Let us first consider the initial and final distributions in Gaussian form,  $p_{XY}^{o/f} = \mathcal{N}(\mathbf{m}^{o/f}, \Sigma^{o/f})$ , which satisfy the following conditions:

$$\begin{cases} m_X^o = m_X^f, \Sigma_{XX}^o \gg \Sigma_{XX}^f \\ m_Y^o = m_Y^f, \Sigma_{YY}^o = \Sigma_{YY}^f \\ \rho_o > \rho_f \geq 0 \end{cases}. \quad (16)$$

These distributions are illustrated in Fig. 3(a). The first condition in Eq. (16) indicates that the variance (fluctuation) of  $X$  is reduced while maintaining the same average. As a result of the second condition, the marginal distribution for  $Y$  remains unchanged throughout the process. Since the mutual information is written in terms of the correlation as  $I_{o/f} = -\frac{1}{2} \ln(1 - \rho_{o/f}^2)$  for Gaussian distributions, the last condition

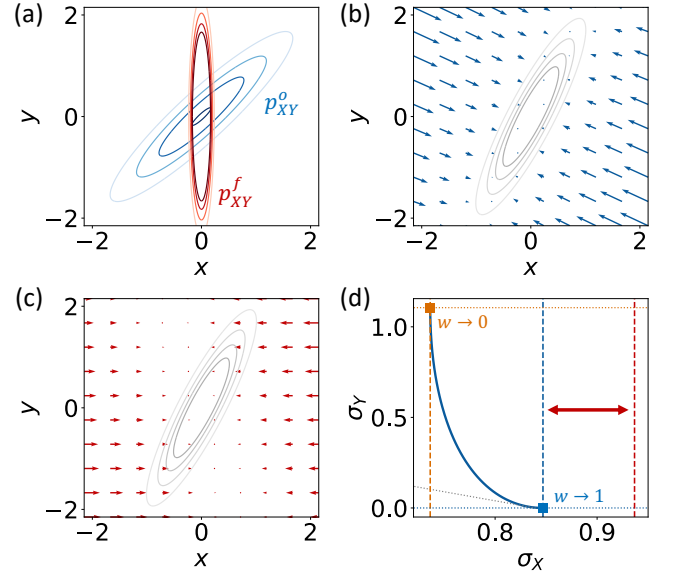


FIG. 3. An optimal Maxwell's demon performing feedback for Gaussian distributions. (a) The initial and final distributions (Eq. (16)). (b)(c) The optimal protocol and distribution (gray contours) at  $t/\tau = 1/2$ . The forces of Eq. (10) at each point are depicted as vectors, where the magnitudes of the forces are represented by the lengths of the vectors. (b) The geodesic term  $T \nabla \ln p_{XY}$  (scaled by  $1/100$ ). (c) The counteradiabatic term  $(\mathbf{r} - \mathbf{r}^o)/\mu t$  (scaled by  $1/10$ ). (d) The optimal cost of feedback (the blue square). The blue curve corresponds to that in (see also Fig. 1) and represents the trade-off relation between  $\sigma_X$  and  $\sigma_Y$ . The vertical dotted lines represent  $\sigma_X^*$  (orange),  $\sigma_X^*|_{\sigma_Y = \sigma_Y^*}$  (blue), and  $-\Delta I$  (red). The red arrow indicates that  $\sigma_X^*|_{\sigma_Y = \sigma_Y^*} < -\Delta I$ , and therefore Maxwell's demon is realized in this protocol (see Eq. (15)). The gray line shows the minimization of the total EP (Eq. (5)). The parameters are set to  $\Sigma_{XX}^o = 1.0$ ,  $\Sigma_{XX}^f = 0.010$ ,  $\Sigma_{YY}^o = \Sigma_{YY}^f = l = 1.0$ ,  $\rho_o = 0.92$ ,  $\rho_f = 0$ ,  $\tau = 1.1$ .

implies that  $Y$ 's information about  $X$  is consumed during the process. We note that this last condition can be replaced by  $\rho_o < \rho_f \leq 0$ . For simplicity, we further assume  $\mathbf{m}^{o/f} = 0$  and  $\rho_f = 0$  in what follows.

We now formulate the optimal feedback process for the distributions in Eq. (16) using Eq. (12). In this process, the engine  $X$  receives feedback to return to  $x \simeq 0$  based on  $Y$ 's record,  $y (\simeq x)$ . The optimal cost of feedback is calculated from Eq. (12) as

$$\sigma_X^*|_{\sigma_Y = \sigma_Y^*} = \sigma_X^* + \frac{2\sqrt{\Sigma_{XX}^o \Sigma_{XX}^f}}{\mu T \tau} (1 - e^{-I_o}). \quad (17)$$

This suggests that greater energetic dissipation is required when  $\tau$  is reduced (faster feedback),  $I_o$  is increased (greater information consumption), or  $\Sigma_{XX}^o$  is increased (longer feedback displacement).

We explain the optimal protocol to achieve Eq. (17). For Gaussian distributions, the optimal transport map  $\mathcal{T}^{*,1}$  is lin-



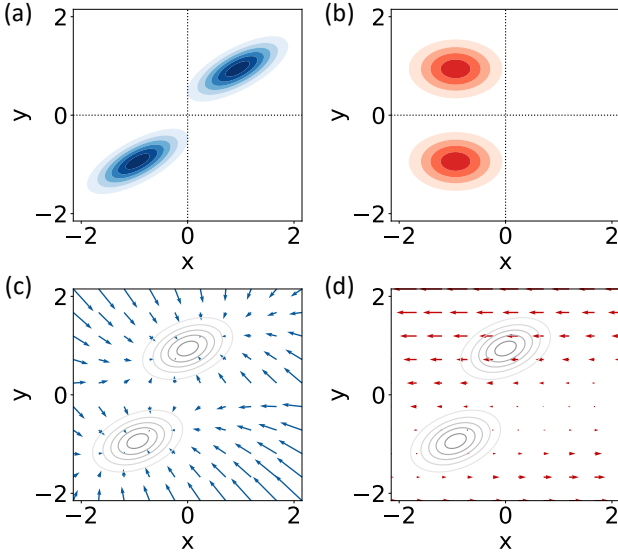


FIG. 4. An optimal Maxwell’s demon performing feedback with the double-well potentials. (a) The initial distribution (Eq. (18)). (b) The final distribution (Eq. (18)). (c)(d) The optimal protocol and distribution (gray contours) at  $t/\tau = 1/2$ . The forces of Eq. (10) at each point are depicted as vectors, where the magnitudes of the forces are represented by the lengths of the vectors. (c) The geodesic term  $T\nabla \ln p_{XY}$  (scaled by  $1/40$ ) (d) The counteradiabatic term  $(\mathbf{r} - \mathbf{r}^o)/\mu t$  (scaled by  $1/4$ ). The parameters are set to  $a = 0.34, b = 0.94, c = 0.35, d = 0.50, l = \sqrt{\text{Var}Y} = 1.0, \tau = 2.2$ .

ear (more precisely, affine). The corresponding protocol is calculated from Eq. (10) and the forces also take the linear form. The nonconservative force comes from the term in the right-hand side of Eq. (10) that has  $y$  dependency. Figure 3(c)(d) illustrates this optimal protocol at the intermediate time  $t/\tau = 1/2$  (see Supplemental Material for details). The counteradiabatic term  $(\mathbf{r} - \mathbf{r}^o)/\mu t$  functions to suppress the fluctuation of  $X$ . For the parameters in Fig. 3, Maxwell’s demon is realized ( $\sigma_X^*|_{\sigma_Y=\sigma_Y^*} = 0.85, -\Delta I = 0.94$ ) and the time limit for the demon is calculated as  $\tau_{\text{demon}} = 0.99l^2/\mu T$ , where  $l := \sqrt{\Sigma_Y^{o/f}}$  denotes the standard deviation of  $Y$ . We set  $\mu = T = 1$  in our numerical calculations.

We note that optimization of finite-time feedback for Gaussian distributions has also been studied in Ref. [37] in a slightly different setup. Their optimal work can be expressed as a special case of Eq. (8), while Eq. (8) applies to general non-Gaussian distributions.

*Non-Gaussian demon with double-well potentials.*— We next demonstrate a non-Gaussian optimal feedback process by Maxwell’s demon using double-well potentials. We consider the following initial and final distributions (see also

Fig. 4(a)(b)):

$$\begin{cases} p^{o/f}(y) \propto \frac{1}{2}e^{-\frac{1}{2a^2}(y-b)^2} + \frac{1}{2}e^{-\frac{1}{2a^2}(y+b)^2} \\ p_{X|Y}^o(x|y) \propto e^{-\frac{1}{2c^2}(x-y)^2}, p_{X|Y}^f(x|y) \propto e^{-\frac{1}{2d^2}(x+b)^2}, \end{cases} \quad (18)$$

where  $a, b, c, d$  are the fixed parameters. The memory  $Y$  is initially located around  $y = \pm b$  and is highly correlated to the engine  $X$ . At the end of this process, the correlation disappears and  $X$  is mainly located around  $x = -b$ . Since the marginal distribution for  $Y$  is identical for  $t = 0$  and  $t = \tau$ , the minimization (8) fixes  $Y$  and implements the optimal feedback process as in the Gaussian case. This feedback moves  $X$  to  $x \simeq -b$  if  $x \simeq b$  initially and keeps  $x \simeq -b$  if  $x \simeq -b$  initially.

The optimal feedback cost is given by Eq. (15) and is calculated as  $\sigma_X^*|_{\sigma_Y=\sigma_Y^*} = [a^2 + 2b^2 + (c-d)^2]/\mu T\tau$ . The optimal map is calculated as  $\mathcal{T}_{X|Y}^*(\mathbf{r}) = \frac{d}{c}(x-y) - b, \mathcal{T}_Y^*(y) = y$ . The optimal protocol is obtained from Eq. (10), as shown in Fig. 4(c)(d). The counteradiabatic term  $(\mathbf{r} - \mathbf{r}^o)/\mu t$  provides feedback to  $X$  to move toward  $x \simeq -b$  when  $y \simeq b$ . For the parameters in Fig. 4, Maxwell’s demon is realized ( $\sigma_X^*|_{\sigma_Y=\sigma_Y^*} = 0.87, -\Delta I = 0.95$ ) and the time limit for the demon is calculated as  $\tau_{\text{demon}} = 2.0l^2/\mu T$ . The time  $\tau_{\text{demon}}$  is nearly twice the Gaussian case, while  $-\Delta I$  remains nearly the same. We note that  $\tau_{\text{demon}}$  can be improved by optimizing the parameters  $a, b, c, d$ .

*Conclusion and perspectives.*— For bipartite overdamped Langevin systems, we derived the fundamental thermodynamic bounds for the partial EPs in finite time (Eqs. (7)(8)). By adopting optimal transport theory, we showed that the bounds are achievable for any time interval and identified the optimal protocol. While our general results apply to non-Gaussian cases (Eq. (8)), the concise formulas are derived for the Gaussian cases (Eq. (12)). Based on our theory, we considered measurement and feedback by Maxwell’s demon and demonstrated optimal feedback processes by the demons for both Gaussian and non-Gaussian models (Figs. 3, 4).

We here make some remarks. First, the optimal EPs (Eqs. (7)(8)) cannot be derived from the continuous limit of the discrete Markov jump case [44]. This is because such limit yields a lower bound of the EP in terms of  $L^1$ , instead of  $L^2$ , Wasserstein distance [24, 25], while the bound given by the  $L^1$ -Wasserstein distance is not achievable in general. Therefore, it is crucial to treat Langevin cases separately from Markov jumps cases. Second, the nonconservative force needs to be manipulated time-dependently in the optimal feedback protocol (Eq. (10)), which would be challenging even with state-of-the-art experimental techniques of optical tweezers [62]. It is an interesting future direction to implement various optimal thermodynamic processes in real experiments, ranging from colloidal particles to biomolecules [63, 64].

*Acknowledgement.*— We thank Kaito Tojo for helpful feedback on the manuscript. This work is supported by JST ERATO Grant Number JPMJER2302, Japan. T.K. is supported by World-leading Innovative Graduate Study Program for Materials Research, Information, and Technology (MERIT-WINGS) of the University of Tokyo. T.K. is also supported by JSPS KAKENHI Grant No. JP24KJ0611. A.T. acknowledges support from JSPS KAKENHI (Grant Nos. 19H05599, and 19K03494). K.F. acknowledges support from JSPS KAKENHI (Grant Nos. JP23K13036 and JP24H00831). T.S. is supported by JSPS KAKENHI Grant No. JP19H05796 and JST CREST Grant No. JPMJCR20C1. T.S. is also supported by Institute of AI and Beyond of the University of Tokyo.

---

\* kamijima@noneq.t.u-tokyo.ac.jp

- [1] H. Leff and A. F. Rex, *Maxwell's Demon 2 Entropy, Classical and Quantum Information, Computing* (CRC Press, 2002).
- [2] J. M. Parrondo, J. M. Horowitz, and T. Sagawa, Thermodynamics of information, *Nature physics* **11**, 131 (2015).
- [3] T. Sagawa and M. Ueda, Second law of thermodynamics with discrete quantum feedback control, *Phys. Rev. Lett.* **100**, 080403 (2008).
- [4] T. Sagawa and M. Ueda, Minimal energy cost for thermodynamic information processing: Measurement and information erasure, *Phys. Rev. Lett.* **102**, 250602 (2009).
- [5] M. Esposito and C. Van den Broeck, Second law and Landauer principle far from equilibrium, *Europhysics Letters* **95**, 40004 (2011).
- [6] T. Sagawa and M. Ueda, Fluctuation theorem with information exchange: Role of correlations in stochastic thermodynamics, *Phys. Rev. Lett.* **109**, 180602 (2012).
- [7] T. Sagawa and M. Ueda, Role of mutual information in entropy production under information exchanges, *New Journal of Physics* **15**, 125012 (2013).
- [8] S. Ito and T. Sagawa, Information thermodynamics on causal networks, *Phys. Rev. Lett.* **111**, 180603 (2013).
- [9] J. M. Horowitz and M. Esposito, Thermodynamics with continuous information flow, *Phys. Rev. X* **4**, 031015 (2014).
- [10] D. Hartich, A. C. Barato, and U. Seifert, Stochastic thermodynamics of bipartite systems: transfer entropy inequalities and a Maxwell's demon interpretation, *Journal of Statistical Mechanics: Theory and Experiment* **2014**, P02016 (2014).
- [11] S. Toyabe, T. Sagawa, M. Ueda, E. Muneyuki, and M. Sano, Experimental demonstration of information-to-energy conversion and validation of the generalized Jarzynski equality, *Nature physics* **6**, 988 (2010).
- [12] A. Bérut, A. Arakelyan, A. Petrosyan, S. Ciliberto, R. Dillenschneider, and E. Lutz, Experimental verification of Landauer's principle linking information and thermodynamics, *Nature* **483**, 187 (2012).
- [13] J. V. Koski, V. F. Maisi, T. Sagawa, and J. P. Pekola, Experimental observation of the role of mutual information in the nonequilibrium dynamics of a Maxwell demon, *Phys. Rev. Lett.* **113**, 030601 (2014).
- [14] M. D. Vidrighin, O. Dahlsten, M. Barbieri, M. S. Kim, V. Vedral, and I. A. Walmsley, Photonic Maxwell's demon, *Phys. Rev. Lett.* **116**, 050401 (2016).
- [15] N. Cottet, S. Jezouin, L. Bretheau, P. Campagne-Ibarcq, Q. Ficheux, J. Anders, A. Auffèves, R. Azouit, P. Rouchon, and B. Huard, Observing a quantum Maxwell demon at work, *Proceedings of the National Academy of Sciences* **114**, 7561 (2017).
- [16] Y. Masuyama, K. Funo, Y. Murashita, A. Noguchi, S. Kono, Y. Tabuchi, R. Yamazaki, M. Ueda, and Y. Nakamura, Information-to-work conversion by Maxwell's demon in a superconducting circuit quantum electrodynamical system, *Nature communications* **9**, 1291 (2018).
- [17] M. Ribezzi-Crivellari and F. Ritort, Large work extraction and the Landauer limit in a continuous Maxwell demon, *Nature Physics* **15**, 660 (2019).
- [18] N. Shiraishi, K. Funo, and K. Saito, Speed limit for classical stochastic processes, *Phys. Rev. Lett.* **121**, 070601 (2018).
- [19] S. Ito, Stochastic thermodynamic interpretation of information geometry, *Phys. Rev. Lett.* **121**, 030605 (2018).
- [20] S. Ito and A. Dechant, Stochastic time evolution, information geometry, and the Cramér-Rao bound, *Phys. Rev. X* **10**, 021056 (2020).
- [21] G. Falasco and M. Esposito, Dissipation-time uncertainty relation, *Phys. Rev. Lett.* **125**, 120604 (2020).
- [22] J. S. Lee, S. Lee, H. Kwon, and H. Park, Speed limit for a highly irreversible process and tight finite-time Landauer's bound, *Phys. Rev. Lett.* **129**, 120603 (2022).
- [23] R. Hamazaki, Speed limits for macroscopic transitions, *PRX Quantum* **3**, 020319 (2022).
- [24] A. Dechant, Minimum entropy production, detailed balance and Wasserstein distance for continuous-time Markov processes, *J. Phys. A* **55**, 094001 (2022).
- [25] T. Van Vu and K. Saito, Thermodynamic unification of optimal transport: Thermodynamic uncertainty relation, minimum dissipation, and thermodynamic speed limits, *Phys. Rev. X* **13**, 011013 (2023).
- [26] R. Sabbagh, O. Movilla Miangolarra, and T. T. Georgiou, Wasserstein speed limits for langevin systems, *Phys. Rev. Res.* **6**, 033308 (2024).
- [27] Y.-H. Ma, R.-X. Zhai, J. Chen, C. P. Sun, and H. Dong, Experimental test of the  $1/\tau$ -scaling entropy generation in finite-time thermodynamics, *Phys. Rev. Lett.* **125**, 210601 (2020).
- [28] A. C. Barato and U. Seifert, Thermodynamic uncertainty relation for biomolecular processes, *Phys. Rev. Lett.* **114**, 158101 (2015).
- [29] T. R. Gingrich, J. M. Horowitz, N. Perunov, and J. L. England, Dissipation bounds all steady-state current fluctuations, *Phys. Rev. Lett.* **116**, 120601 (2016).
- [30] P. Pietzonka, A. C. Barato, and U. Seifert, Universal bounds on current fluctuations, *Phys. Rev. E* **93**, 052145 (2016).
- [31] N. Shiraishi, K. Saito, and H. Tasaki, Universal trade-off relation between power and efficiency for heat engines, *Phys. Rev. Lett.* **117**, 190601 (2016).
- [32] K. Proesmans and C. Van den Broeck, Discrete-time thermodynamic uncertainty relation, *EPL* **119**, 20001 (2017).
- [33] P. Pietzonka and U. Seifert, Universal trade-off between power,

- efficiency, and constancy in steady-state heat engines, *Phys. Rev. Lett.* **120**, 190602 (2018).
- [34] Y. Hasegawa and T. Van Vu, Uncertainty relations in stochastic processes: An information inequality approach, *Phys. Rev. E* **99**, 062126 (2019).
- [35] T. Koyuk and U. Seifert, Thermodynamic uncertainty relation for time-dependent driving, *Phys. Rev. Lett.* **125**, 260604 (2020).
- [36] K. Liu, Z. Gong, and M. Ueda, Thermodynamic uncertainty relation for arbitrary initial states, *Phys. Rev. Lett.* **125**, 140602 (2020).
- [37] D. Abreu and U. Seifert, Extracting work from a single heat bath through feedback, *Europhysics Letters* **94**, 10001 (2011).
- [38] K. Proesmans, J. Ehrich, and J. Bechhoefer, Finite-time Landauer principle, *Phys. Rev. Lett.* **125**, 100602 (2020).
- [39] Y.-Z. Zhen, D. Egloff, K. Modi, and O. Dahlsten, Universal bound on energy cost of bit reset in finite time, *Phys. Rev. Lett.* **127**, 190602 (2021).
- [40] M. Nakazato and S. Ito, Geometrical aspects of entropy production in stochastic thermodynamics based on Wasserstein distance, *Phys. Rev. Res.* **3**, 043093 (2021).
- [41] A. Taghvaei, O. M. Miangolarra, R. Fu, Y. Chen, and T. T. Georgiou, On the relation between information and power in stochastic thermodynamic engines, *IEEE Control Systems Letters* **6**, 434 (2022).
- [42] R. Nagase and T. Sagawa, Thermodynamically optimal information gain in finite-time measurement, *Phys. Rev. Res.* **6**, 033239 (2024).
- [43] Y. Fujimoto and S. Ito, Game-theoretical approach to minimum entropy productions in information thermodynamics, *Phys. Rev. Res.* **6**, 013023 (2024).
- [44] T. Kamijima, K. Funo, and T. Sagawa, Finite-time thermodynamic bounds and tradeoff relations for information processing, *arXiv preprint arXiv:2409.08606* (2024).
- [45] S. Dago, J. Pereda, N. Barros, S. Ciliberto, and L. Bellon, Information and thermodynamics: Fast and precise approach to Landauer's bound in an underdamped micromechanical oscillator, *Phys. Rev. Lett.* **126**, 170601 (2021).
- [46] C. Villani, *Topics in Optimal Transportation*, 58 (American Mathematical Soc., 2003).
- [47] C. Villani, *Optimal transport: old and new*, Vol. 338 (Springer, 2009).
- [48] F. Santambrogio, *Optimal transport for applied mathematicians*, Birkhäuser, NY **55**, 94 (2015).
- [49] N. G. Van Kampen, *Stochastic processes in physics and chemistry*, Vol. 1 (Elsevier, 1992).
- [50] U. Seifert, Stochastic thermodynamics, fluctuation theorems and molecular machines, *Rep. Prog. Phys.* **75**, 126001 (2012).
- [51] A. E. Allahverdyan, D. Janzing, and G. Mahler, Thermodynamic efficiency of information and heat flow, *Journal of Statistical Mechanics: Theory and Experiment* **2009**, P09011 (2009).
- [52] M. L. Rosinberg and J. M. Horowitz, Continuous information flow fluctuations, *Europhysics Letters* **116**, 10007 (2016).
- [53] E. Aurell, C. Mejía-Monasterio, and P. Muratore-Ginanneschi, Optimal protocols and optimal transport in stochastic thermodynamics, *Phys. Rev. Lett.* **106**, 250601 (2011).
- [54] E. Aurell, K. Gawędzki, C. Mejía-Monasterio, R. Mohayaei, and P. Muratore-Ginanneschi, Refined second law of thermodynamics for fast random processes, *Journal of statistical physics* **147**, 487 (2012).
- [55] J.-D. Benamou and Y. Brenier, A computational fluid mechanics solution to the Monge-Kantorovich mass transfer problem, *Numerische Mathematik* **84**, 375 (2000).
- [56] A. Dechant and Y. Sakurai, Thermodynamic interpretation of Wasserstein distance, *arXiv preprint arXiv:1912.08405* (2019).
- [57] Y. Chen, T. T. Georgiou, and A. Tannenbaum, Stochastic control and nonequilibrium thermodynamics: Fundamental limits, *IEEE Transactions on Automatic Control* **65**, 2979 (2020).
- [58] K. Proesmans, Precision-dissipation trade-off for driven stochastic systems, *Communications Physics* **6**, 226 (2023).
- [59] P. Abiuso, V. Holubec, J. Anders, Z. Ye, F. Cerisola, and M. Perarnau-Llobet, Thermodynamics and optimal protocols of multidimensional quadratic brownian systems, *Journal of Physics Communications* **6**, 063001 (2022).
- [60] See supplemental material at.
- [61] A. Zhong and M. R. DeWeese, Beyond linear response: Equivalence between thermodynamic geometry and optimal transport, *Phys. Rev. Lett.* **133**, 057102 (2024).
- [62] S. Sukhov and A. Dogariu, Non-conservative optical forces, *Reports on Progress in Physics* **80**, 112001 (2017).
- [63] T. K. Saha, J. N. E. Lucero, J. Ehrich, D. A. Sivak, and J. Bechhoefer, Bayesian information engine that optimally exploits noisy measurements, *Phys. Rev. Lett.* **129**, 130601 (2022).
- [64] K. W. Tang, K. J. Ray, and J. P. Crutchfield, Nonequilibrium thermodynamics of a superconducting Szilard engine, *arXiv preprint arXiv:2407.20418* (2024).

# Supplemental Material for “Finite-time optimal Maxwell’s Demons”

## S1. REVIEW OF STOCHASTIC THERMODYNAMICS

First, we briefly review stochastic thermodynamics of overdamped Langevin systems (Eqs. (1)(2)). The rates of the absorbed heat and extracted work are defined as [1]

$$\dot{Q} := - \int d\mathbf{r} (-\nabla V(\mathbf{r}, t) + \mathbf{F}(\mathbf{r}, t))^T \mathbf{v}(\mathbf{r}, t) p_{XY}(\mathbf{r}, t), \quad (\text{S1})$$

$$\dot{W}_{\text{ext}} := \int d\mathbf{r} (-\partial_t V(\mathbf{r}, t) - \mathbf{F}(\mathbf{r}, t)^T \mathbf{v}(\mathbf{r}, t)) p_{XY}(\mathbf{r}, t). \quad (\text{S2})$$

The average energy of the system is given by  $E := \int d\mathbf{r} V(\mathbf{r}, t) p_{XY}(\mathbf{r}, t)$ , leading to the first law of thermodynamics  $d_t E = -\dot{W}_{\text{ext}} + \dot{Q}$ . By using the Shannon entropy of the total system

$$S_{XY} := - \int d\mathbf{r} p_{XY}(\mathbf{r}, t) \ln p_{XY}(\mathbf{r}, t), \quad (\text{S3})$$

the entropy production rate of the total system [Eq. (3) of the main text] is given by

$$\dot{\sigma}_{XY} = d_t S_{XY} - \frac{\dot{Q}}{T}. \quad (\text{S4})$$

By introducing the nonequilibrium free energy

$$\mathcal{F}_{XY} := E - TS_{XY}, \quad (\text{S5})$$

the entropy production rate is rewritten as

$$\dot{\sigma}_{XY} = \frac{-\dot{W}_{\text{ext}} - d_t \mathcal{F}_{XY}}{T}. \quad (\text{S6})$$

In bipartite systems, the mutual information between subsystems is defined as [2]

$$I := \int d\mathbf{r} p_{XY}(\mathbf{r}, t) \ln \frac{p_{XY}(\mathbf{r}, t)}{p_X(x, t) p_Y(y, t)}. \quad (\text{S7})$$

The change of  $I$  can be decomposed into the contributions of the subsystems [3, 4]:

$$d_t I = \dot{I}_X + \dot{I}_Y, \quad (\text{S8})$$

$$\dot{I}_X := \int d\mathbf{r} p_{XY}(\mathbf{r}, t) v_X(\mathbf{r}, t) \partial_x \ln \frac{p_{XY}(\mathbf{r}, t)}{p_X(x, t) p_Y(y, t)}, \quad (\text{S9})$$

$$\dot{I}_Y := \int d\mathbf{r} p_{XY}(\mathbf{r}, t) v_Y(\mathbf{r}, t) \partial_y \ln \frac{p_{XY}(\mathbf{r}, t)}{p_X(x, t) p_Y(y, t)}, \quad (\text{S10})$$

where  $\dot{I}_X$  ( $\dot{I}_Y$ ) is called the information flow and provides the information gain or loss induced by the change of  $X$  ( $Y$ ). The entropy production rate of the subsystem  $X$  (Eq. (4)) is written as

$$\dot{\sigma}_X = d_t S_X - \frac{\dot{Q}_X}{T} - \dot{I}_X, \quad (\text{S11})$$

where  $S_X := - \int dx p_X(x, t) \ln p_X(x, t)$  is the Shannon entropy of  $X$  and  $\dot{Q}_X := - \int d\mathbf{r} (-\partial_x V(\mathbf{r}, t) + F_X(\mathbf{r}, t)) v_X(\mathbf{r}, t) p_{XY}(\mathbf{r}, t)$  is the heat absorbed by  $X$ . In the special case that the other subsystem  $Y$  does not evolve as in the feedback process, the EP of  $X$  is expressed using the work:

$$\dot{\sigma}_X = \dot{\sigma}_{XY} = \frac{-\dot{W}_{\text{ext}} - d_t \mathcal{F}_X}{T} - d_t I, \quad (\text{S12})$$

where  $\mathcal{F}_X := E - TS_X$  is the nonequilibrium energy of the subsystem  $X$ . The same definitions and formulas also apply to the subsystem  $Y$  by exchanging  $X$  and  $Y$ .



## S2. THE OPTIMAL FEEDBACK PROTOCOL

In this section, we explain the optimal map and the optimal protocol for the finite-time feedback in Figs. 3,4.

### A. The Gaussian Case

#### 1. The optimal map

We here consider general Gaussian distributions  $p_{XY}^{o/f} = \mathcal{N}(\mathbf{m}^{o/f}, \Sigma^{o/f})$  for illustration, while Fig. 3 assumes a specific form of distributions expressed in Eq. (16). Although the optimal maps for  $X$  and  $Y$  can be calculated using the cumulative distribution functions, as stated in the main text, here we leverage the fact that if a one-dimensional transport map has a non-decreasing linear form then it is optimal [5]. We first explicitly present the optimal transport map for  $Y$ , assumed to be  $\mathcal{T}_Y^*(y) := a_Y y + b_Y$  ( $a_Y \geq 0$ ). Since the marginal distribution for  $Y$  is transported by this map as

$$p_Y^f(y) = \int dy^o \delta(y - (a_Y y^o + b_Y)) p_Y^o(y^o) = \frac{1}{a_Y} p_Y^o\left(\frac{y - b_Y}{a_Y}\right), \quad (\text{S13})$$

the constants  $a_Y$  and  $b_Y$  are calculated as  $a_Y = \sqrt{\Sigma_{YY}^f / \Sigma_{YY}^o}$  and  $b_Y = m_Y^f - a_Y m_Y^o$ , respectively. Thus, the optimal map for  $Y$  is given by

$$\mathcal{T}_Y^*(y) = \sqrt{\frac{\Sigma_{YY}^f}{\Sigma_{YY}^o}} (y - m_Y^o) + m_Y^f. \quad (\text{S14})$$

We next construct the  $X$  component of the transport map, assumed to be  $\mathcal{T}_{X|Y}^*(x; y) := a_X x + b_X$  ( $a_X \geq 0$ ). The conditional distributions of  $X$  given  $Y = y$  are

$$p_{X|Y}^{o/f}(x|y) = \sqrt{\frac{\Sigma_{YY}^{o/f}}{2\pi \det \Sigma^{o/f}}} \exp \left[ -\frac{\Sigma_{YY}^{o/f}}{2 \det \Sigma^{o/f}} \left( x - m_X^{o/f} - \frac{\Sigma_{XY}^{o/f}}{\Sigma_{YY}^{o/f}} (y - m_Y^{o/f}) \right)^2 \right]. \quad (\text{S15})$$

Since  $p_{X|Y}^o(\cdot|y)$  is transported to  $p_{X|Y}^f(\cdot|\mathcal{T}_Y^*(y))$  by the map  $\mathcal{T}_{X|Y}^*$ ,

$$p_{X|Y}^f(x|\mathcal{T}_Y^*(y)) = \int dx^o \delta(x - (a_X x^o + b_X)) p_{X|Y}^o(x^o|y) = \frac{1}{a_X} p_{X|Y}^o\left(\frac{x - b_X}{a_X} | y\right) \quad (\text{S16})$$

holds. The constants  $a_X$  and  $b_X$  are determined by comparison, yielding the transport map for  $X$  as

$$\begin{aligned} \mathcal{T}_{X|Y}^*(x; y) &= \sqrt{\frac{\det \Sigma^f}{\Sigma_{YY}^f \det \Sigma^o}} \left( x - m_X^o - \frac{\Sigma_{XY}^o}{\Sigma_{YY}^o} (y - m_Y^o) \right) + m_X^f + \frac{\Sigma_{XY}^f}{\Sigma_{YY}^f} \left( \sqrt{\frac{\Sigma_{YY}^f}{\Sigma_{YY}^o}} (y - m_Y^o) + m_Y^f - m_Y^o \right) \\ &= \sqrt{\frac{1 - \rho_f^2}{1 - \rho_o^2} \frac{\Sigma_{XX}^f}{\Sigma_{XX}^o}} (x - m_X^o) + \left( \rho_f - \rho_o \sqrt{\frac{1 - \rho_f^2}{1 - \rho_o^2}} \right) \sqrt{\frac{\Sigma_{XX}^f}{\Sigma_{YY}^o}} (y - m_Y^o) + m_X^f. \end{aligned} \quad (\text{S17})$$

To summarize, the optimal transport map to achieve Eq. (12) is represented as

$$\mathcal{T}^{*,1}(\mathbf{r}) = G_1(\mathbf{r} - \mathbf{m}^o) + \mathbf{m}^f, \quad (\text{S18})$$

$$G_1 = \begin{bmatrix} \sqrt{\frac{1 - \rho_f^2}{1 - \rho_o^2} \frac{\Sigma_{XX}^f}{\Sigma_{XX}^o}} & \left( \rho_f - \rho_o \sqrt{\frac{1 - \rho_f^2}{1 - \rho_o^2}} \right) \sqrt{\frac{\Sigma_{XX}^f}{\Sigma_{YY}^o}} \\ 0 & \sqrt{\frac{\Sigma_{YY}^f}{\Sigma_{YY}^o}} \end{bmatrix}. \quad (\text{S19})$$

## 2. The optimal protocol

We next construct the optimal protocol from the obtained optimal map (Eq. (S18)). We set  $\Sigma_{YY}^o = \Sigma_{YY}^f$ ,  $\mathbf{m}^{o/f} = 0$ , and  $\rho_f = 0$  as in the main text. The Lagrange map is given by  $\mathcal{T}^{*,1}(\mathbf{r}, t) = (1 - t/\tau)\mathbf{r} + (t/\tau)\mathcal{T}^{*,1}(\mathbf{r}) = ((1 - t/\tau)\mathbf{1} + (t/\tau)G_1)\mathbf{r}$ , with  $\mathbf{1}$  being the  $2 \times 2$  identity matrix. The covariance matrix at time  $t$  is written as

$$\Sigma(t) = \left( \left( 1 - \frac{t}{\tau} \right) \mathbf{1} + \frac{t}{\tau} G_1 \right) \Sigma^o \left( \left( 1 - \frac{t}{\tau} \right) \mathbf{1} + \frac{t}{\tau} G_1 \right)^T. \quad (\text{S20})$$

The boundary condition  $\Sigma(\tau) = \Sigma^f$  is verified by  $G_1 \Sigma^o G_1^T = \Sigma^f$ . The right-hand side of Eq. (10) is calculated as follows:

$$\begin{aligned} \mathbf{r}^o &= \left( \left( 1 - \frac{t}{\tau} \right) \mathbf{1} + \frac{t}{\tau} G_1 \right)^{-1} \mathbf{r} \\ &= \begin{bmatrix} \frac{1}{1 - \frac{t}{\tau} + \frac{t}{\tau} \sqrt{\Sigma_{XX}^f / (1 - \rho_o^2) \Sigma_{XX}^o}} & \frac{\frac{t}{\tau} \rho_o \sqrt{\Sigma_{XX}^f / (1 - \rho_o^2) \Sigma_{YY}^o}}{1 - \frac{t}{\tau} + \frac{t}{\tau} \sqrt{\Sigma_{XX}^f / (1 - \rho_o^2) \Sigma_{XX}^o}} \\ 0 & 1 \end{bmatrix} \mathbf{r}, \end{aligned} \quad (\text{S21})$$

$$\frac{\mathbf{r} - \mathbf{r}^o}{t} = \begin{bmatrix} \frac{-\tau^{-1}}{1 - \frac{t}{\tau} + \frac{t}{\tau} \sqrt{\Sigma_{XX}^f / (1 - \rho_o^2) \Sigma_{XX}^o}} & \left( \left( 1 - \sqrt{\Sigma_{XX}^f / (1 - \rho_o^2) \Sigma_{XX}^o} \right) x + \rho_o \sqrt{\Sigma_{XX}^f / (1 - \rho_o^2) \Sigma_{YY}^o} y \right) \\ 0 & \end{bmatrix}. \quad (\text{S22})$$

The nonconservative force is required to implement the term of  $y$  in Eq. (S22). The optimal protocol is depicted in Fig. 3(a) and (b).

## B. The Double-Well Case

### 1. The optimal map

We consider the distributions expressed in Eq. (18). Since the marginal distribution of  $Y$  is identical at  $t = 0$  and  $t = \tau$ , the optimal transport for  $Y$  is simply  $\mathcal{T}_Y^*(y) = y$ . The cumulative distribution functions of  $p_{X|Y}^{o/f}$  are given by

$$\Gamma_{X|Y}^o(x; y) = \Gamma\left(\frac{1}{c}(x - y)\right), \Gamma_{X|Y}^f(x; y) = \Gamma\left(\frac{1}{d}(x + b)\right), \quad (\text{S23})$$

where  $\Gamma(x) := \int_{-\infty}^x dx' \exp(-x'^2/2)/\sqrt{2\pi}$  represents the cumulative distribution function of the normal distribution. The inverse function of  $\Gamma_{X|Y}^f$  with respect to  $x$  is

$$\Gamma_{X|Y}^f{}^{-1}(s; y) = d \Gamma^{-1}(s) - b, \quad (\text{S24})$$

where  $\Gamma^{-1}$  denotes the inverse function of  $\Gamma$ . From Eq. (9), the  $X$  component of optimal transport map is obtained as

$$\mathcal{T}_{X|Y}^*(x; y) = \Gamma_{X|Y}^f{}^{-1}\left(\Gamma_{X|Y}^o(x; y); \mathcal{T}_Y^*(y)\right) = \frac{d}{c}(x - y) - b. \quad (\text{S25})$$

### 2. The optimal protocol

We construct the optimal protocol from  $\mathcal{T}_Y^*(y) = y$  and Eq. (S25). The probability distribution evolves to

$$p_{XY}(\mathbf{r}, t) = \int d\mathbf{r}^o \delta(\mathbf{r} - \mathcal{T}^{*,1}(\mathbf{r}^o, t)) p_{XY}^o(\mathbf{r}^o) = \frac{1}{(1 - \frac{t}{\tau}) + \frac{t}{\tau} \frac{d}{c}} p_{X|Y}^o\left(\frac{x + \frac{t}{\tau}(\frac{d}{c}y + b)}{(1 - \frac{t}{\tau}) + \frac{t}{\tau} \frac{d}{c}} \middle| y\right) p_Y^o(y) \quad (\text{S26})$$

at time  $t$ , where  $\mathcal{T}^{*,1}(\mathbf{r}^o, t)$  is the Lagrange map in Eq. (10). The right-hand side of Eq. (10) is calculated as

$$\mathbf{r} = \mathcal{T}^{*,1}(\mathbf{r}^o, t) = \begin{bmatrix} (1 - \frac{t}{\tau})x^o + \frac{t}{\tau} \frac{d}{c}(x^o - y^o) - \frac{t}{\tau} b \\ y^o \end{bmatrix}, \quad (\text{S27})$$

$$\frac{\mathbf{r} - \mathbf{r}^o}{t} = \begin{bmatrix} \frac{-1}{\tau} \frac{(1 - \frac{d}{c})x + b + \frac{d}{c}y}{(1 - \frac{t}{\tau}) + \frac{t}{\tau} \frac{d}{c}} \\ 0 \end{bmatrix}. \quad (\text{S28})$$

The nonconservative force is required to implement the term of  $y$  in Eq. (S28). The optimal protocol is depicted in Fig. 4(c) and (d).

### S3. PROOFS OF THE MAIN RESULTS

In this section, we prove the main results of the main texts. In what follows, we always assume that all functions and maps are regular enough to justify our computation.

#### A. Proof of Eq. (7)

To begin with, we change the variable from the velocity field  $\{\mathbf{v}\}_{0 \leq t \leq \tau}$  to the Lagrange map  $\{\mathcal{T}\}_{0 \leq t \leq \tau}$  that realizes  $p_{XY}^o \rightarrow p_{XY}^f$ . This map satisfies  $\partial_t \mathcal{T}(\mathbf{r}, t) = \mathbf{v}(\mathcal{T}(\mathbf{r}, t), t)$ , with the initial condition  $\mathcal{T}(\mathbf{r}, 0) = \mathbf{r}$  and the final condition  $\mathcal{T}(\mathbf{r}, \tau) = \mathcal{T}^f(\mathbf{r})$ , where  $\mathcal{T}^f$  (denoted as  $\mathcal{T}$  in the main text) is a transport map from  $p_{XY}^o$  to  $p_{XY}^f$ . Then, the EP of  $Y$  is evaluated as

$$\begin{aligned} \sigma_Y &= \frac{1}{\mu T} \int_0^\tau dt \int d\mathbf{r} v_Y(\mathbf{r}, t)^2 p_{XY}(\mathbf{r}, t) \\ &= \frac{1}{\mu T} \int_0^\tau dt \int d\mathbf{r}^o (\partial_t \mathcal{T}_Y(\mathbf{r}^o, t))^2 p_{XY}^o(\mathbf{r}^o) \\ &\geq \frac{1}{\mu T \tau} \int d\mathbf{r}^o \left( \mathcal{T}_Y^f(\mathbf{r}^o) - y^o \right)^2 p_{XY}^o(\mathbf{r}^o). \end{aligned} \quad (\text{S29})$$

In the last inequality, using the method of Lagrange multipliers, the form of the optimal map is specified as the interpolation  $\mathcal{T}(\mathbf{r}, t) = (1 - t/\tau)\mathbf{r} + (t/\tau)\mathcal{T}^f(\mathbf{r})$ . If we substitute  $\mathcal{T}^f(\mathbf{r}) = [\mathcal{T}_{X|Y}^f(x; y), \mathcal{T}_Y^*(y)]^T$  into Eq. (S29), the rightmost of Eq. (7) is obtained. Here,  $\mathcal{T}_Y^*(y) = \Gamma_Y^{f^{-1}}(\Gamma_Y^o(y))$  is the one-dimensional optimal map for  $Y$ . The  $X$  component of optimal transport map,  $\mathcal{T}_{X|Y}^f(x; y)$ , that realizes the transport  $p_{XY}^o \rightarrow p_{XY}^f$  is provided by e.g., the Knothe–Rosenblatt map,  $\mathcal{T}_{X|Y}^f(x; y) = \mathcal{T}_{X|Y}^*(x; y) = \Gamma_{X|Y}^{f^{-1}}(\Gamma_{X|Y}^o(x; y; \mathcal{T}_Y^*(y)))$ . We conclude that Eq. (7) is proved because the marginal Wasserstein distance  $\mathcal{W}(p_Y^o, p_Y^f)$  also gives the lower bound of  $\sigma_Y$  [6]. The Lagrange map for  $X$ ,  $\mathcal{T}_{X|Y}(x, t; y)$ , is freely determined as long as continuously connecting  $x$  and  $\mathcal{T}_{X|Y}^f(x; y)$  in time.

The above proof does not exclude the existence of a transport map  $\mathcal{T}^f$  that realizes  $p_{XY}^o \rightarrow p_{XY}^f$ , where  $\mathcal{T}_Y^f$  depends on  $x$  and the minimum EP (Eq. (7)) is attained. We however prove that such a map does not exist in general. We consider the following Lagrangian:

$$\mathcal{L}[\mathcal{T}^f] := \frac{1}{2} \int d\mathbf{r}^o \left( \mathcal{T}_Y^f(\mathbf{r}^o) - y^o \right)^2 p_{XY}^o(\mathbf{r}^o) + \int d\mathbf{r}^f \lambda(\mathbf{r}^f) \left[ \int d\mathbf{r}^o \delta(\mathbf{r}^f - \mathcal{T}^f(\mathbf{r}^o)) p_{XY}^o(\mathbf{r}^o) - p_{XY}^f(\mathbf{r}^f) \right], \quad (\text{S30})$$

where  $\lambda(\mathbf{r}^f)$  represents the Lagrange multiplier. The variation of the Lagrangian is calculated as

$$\delta \mathcal{L} = \int d\mathbf{r}^f [\partial_{x^f} \lambda(\mathbf{r}^f)] \delta \mathcal{T}_X^f(\mathcal{T}^o(\mathbf{r}^f)) p_{XY}^f(\mathbf{r}^f) + \int d\mathbf{r}^f [\partial_{y^f} \lambda(\mathbf{r}^f) + y^f - \mathcal{T}_Y^o(\mathbf{r}^f)] \delta \mathcal{T}_Y^f(\mathcal{T}^o(\mathbf{r}^f)) p_{XY}^f(\mathbf{r}^f), \quad (\text{S31})$$

where  $\mathcal{T}^o := \mathcal{T}^{f^{-1}}$  denotes the inverse function of the transport map  $\mathcal{T}^f$ . From the variation  $\delta \mathcal{T}_X^f(\mathcal{T}^o(\mathbf{r}^f))$ , the Lagrange multiplier must be independent of  $x$ . Similarly, from the variation  $\delta \mathcal{T}_Y^f(\mathcal{T}^o(\mathbf{r}^f))$ , the  $Y$  component of the optimal map must also be independent of  $x$ .

#### B. Proof of Eq. (8)

We first minimize the EP of  $Y$  according to Sec. S3 A. The components of the Lagrange map  $\mathcal{T}(\mathbf{r}, t)$  satisfy  $\mathcal{T}_Y(\mathbf{r}, t) = (1 - t/\tau)y + (t/\tau)\mathcal{T}_Y^*(y)$  and  $\mathcal{T}_X(\mathbf{r}, 0) = x$ ,  $\mathcal{T}_X(\mathbf{r}, \tau) = \mathcal{T}_{X|Y}(x; y)$ . We next consider minimizing the EP of  $X$  under this

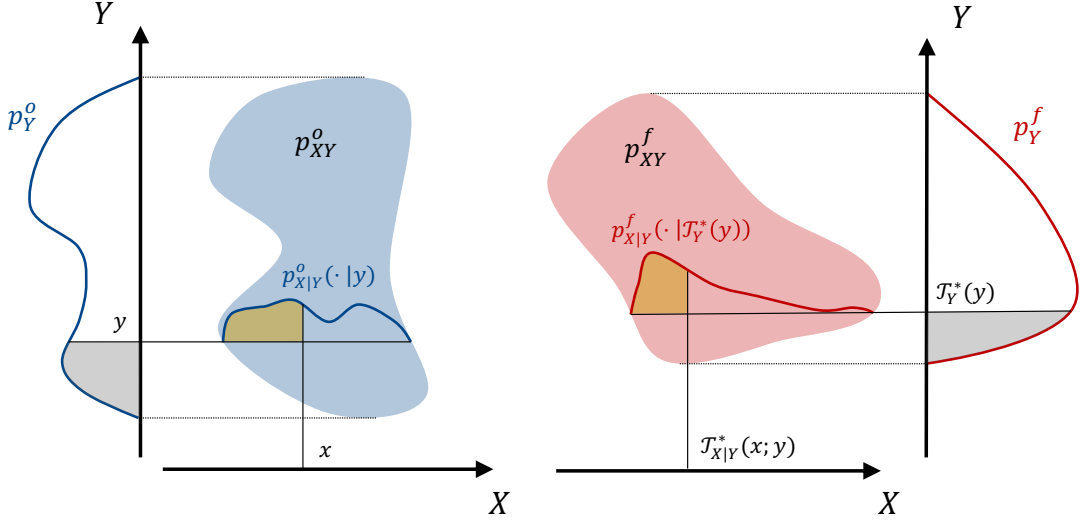


FIG. S1. The optimal map to realize Eq. (8). The areas of the shaded regions are identical, respectively for gray and yellow. This map is known as Knothe–Rosenblatt map [7].

condition. The EP of  $X$  is

$$\begin{aligned}
 \sigma_X &= \frac{1}{\mu T} \int_0^\tau dt \int d\mathbf{r} (\partial_t \mathcal{T}_X(\mathbf{r}, t))^2 p_{XY}^o(\mathbf{r}) \\
 &\geq \frac{1}{\mu T \tau} \int d\mathbf{r} (\mathcal{T}_{X|Y}(x; y) - x)^2 p_{XY}^o(\mathbf{r}) \\
 &= \frac{1}{\mu T \tau} \int dy p_Y^o(y) \int dx (\mathcal{T}_{X|Y}(x; y) - x)^2 p_{X|Y}^o(x|y),
 \end{aligned} \tag{S32}$$

where we used the same reasoning as in Eq. (S29) to obtain the inequality in Eq. (S32).

We explain the constraint on the map  $\mathcal{T}_{X|Y}$ . The Jacobian equations (completeness of transport) of  $\mathcal{T}_Y^*(y)$  and  $\mathcal{T}(\mathbf{r}) = [\mathcal{T}_{X|Y}(x; y), \mathcal{T}_Y^*(y)]^T$  are given by

$$p_Y^o(y) = \frac{\partial \mathcal{T}_Y^*(y)}{\partial y} p_Y^f(\mathcal{T}_Y^*(y)), \tag{S33}$$

$$p_{XY}^o(\mathbf{r}) = \left| \det \frac{\partial \mathcal{T}(\mathbf{r})}{\partial \mathbf{r}} \right| p_{XY}^f(\mathcal{T}(\mathbf{r})) = \frac{\partial \mathcal{T}_Y^*(y)}{\partial y} \frac{\partial \mathcal{T}_{X|Y}(x; y)}{\partial x} p_{XY}^f(\mathcal{T}(\mathbf{r})). \tag{S34}$$

We then obtain the Jacobian equation of  $\mathcal{T}_{X|Y}(x; y)$  by dividing Eq. (S34) with Eq. (S33) as

$$p_{X|Y}^o(x|y) = \frac{\partial \mathcal{T}_{X|Y}(x; y)}{\partial x} p_{X|Y}^f(\mathcal{T}_{X|Y}(x; y) | \mathcal{T}_Y^*(y)). \tag{S35}$$

This indicates that the map  $\mathcal{T}_{X|Y}(\cdot; y)$  realizes the one-dimensional transport from  $p_{X|Y}^o(\cdot|y)$  to  $p_{X|Y}^f(\cdot | \mathcal{T}_Y^*(y))$ . Combining Eq. (S32) and Eq. (S35), the EP of  $X$  is minimized if  $p_{X|Y}^o(\cdot|y)$  is transported optimally to  $p_{X|Y}^f(\cdot | \mathcal{T}_Y^*(y))$  for all  $y$ . For each  $y$ , the optimal transport cost equals the square of the Wasserstein distance between the conditional distributions, providing Eq. (8). Since this is the transport of one-dimensional distributions, the optimal transport map is given by Eq. (9). This map is illustrated in Fig. S1.

### C. Derivation of Eq. (12)

Using Eqs. (8)(11)(S14)(S15),  $\sigma_X^*|_{\sigma_Y=\sigma_Y^*}$  is calculated as

$$\begin{aligned}
\sigma_X^*|_{\sigma_Y=\sigma_Y^*} &= \frac{1}{\mu T \tau} \int dy p_Y^o(y) \left[ \left( \left( m_X^o + \frac{\Sigma_{XY}^o}{\Sigma_{YY}^o} (y - m_Y^o) \right) - \left( m_X^f + \frac{\Sigma_{XY}^f}{\Sigma_{YY}^f} \left( \sqrt{\frac{\Sigma_{YY}^f}{\Sigma_{YY}^o}} (y - m_Y^o) + m_Y^f - m_Y^f \right) \right) \right)^2 \right] \\
&\quad + \frac{1}{\mu T \tau} \left( \sqrt{\frac{\det \Sigma^o}{\Sigma_{YY}^o}} - \sqrt{\frac{\det \Sigma^f}{\Sigma_{YY}^f}} \right)^2 \\
&= \frac{1}{\mu T \tau} \left[ (m_X^o - m_X^f)^2 + \left( \frac{\Sigma_{XY}^o}{\Sigma_{YY}^o} - \frac{\Sigma_{XY}^f}{\sqrt{\Sigma_{YY}^o \Sigma_{YY}^f}} \right)^2 \Sigma_{YY}^o + \left( \sqrt{\frac{\det \Sigma^o}{\Sigma_{YY}^o}} - \sqrt{\frac{\det \Sigma^f}{\Sigma_{YY}^f}} \right)^2 \right] \\
&= \frac{1}{\mu T \tau} \left[ \mathcal{W}(p_X^o, p_X^f)^2 + 2 \left( \sqrt{\Sigma_{XX}^o \Sigma_{XX}^f} - \frac{\Sigma_{XY}^o \Sigma_{XY}^f}{\sqrt{\Sigma_{YY}^o \Sigma_{YY}^f}} - \sqrt{\frac{\det \Sigma^o \det \Sigma^f}{\Sigma_{YY}^o \Sigma_{YY}^f}} \right) \right] \\
&= \sigma_X^* + \frac{2\sqrt{\Sigma_{XX}^o \Sigma_{XX}^f}}{\mu T \tau} \left( 1 - \rho_o \rho_f - \sqrt{(1 - \rho_o^2)(1 - \rho_f^2)} \right). \tag{S36}
\end{aligned}$$

Thus, Eq. (12) is derived.

## S4. PARETO FRONT

In this section, we consider the Pareto front of the partial EPs for overdamped Langevin systems, which is represented by the blue curve of Fig. 1. We note that the Pareto front has also been considered for discrete Markov jump systems in Ref. [8], which however has a very different structure from the Langevin case.

### A. Definitions and General Results

The tradeoff relation between incompatible  $\sigma_X$  and  $\sigma_Y$  can be described by the set of their optimal pair, called the Pareto front [9, 10]. On the Pareto front (denoted as  $\mathcal{P}$ ),  $\sigma_X$  cannot be decreased without increasing  $\sigma_Y$ , and vice versa (see Fig. 1). Let us define the feasible region  $\mathcal{K}$  as the set of all pairs implemented by some protocols  $\{V, F\}_{0 \leq t \leq \tau}$  that realize  $p_{XY}^o \rightarrow p_{XY}^f$ . If there exists a feasible pair  $(\sigma_X', \sigma_Y') \in \mathcal{K}$  such that

$$\sigma_X' < \sigma_X, \sigma_Y' \leq \sigma_Y \text{ or } \sigma_X' \leq \sigma_X, \sigma_Y' < \sigma_Y, \tag{S37}$$

then the pair  $(\sigma_X, \sigma_Y)$  is not included in  $\mathcal{P}$ . This relation between such pairs is denoted as  $(\sigma_X', \sigma_Y') \prec (\sigma_X, \sigma_Y)$ . Then, the Pareto front  $\mathcal{P}$  can be more explicitly defined as

$$\mathcal{P} := \{(\sigma_X, \sigma_Y) \in \mathcal{K} \mid \forall (\sigma_X', \sigma_Y') \in \mathcal{K}, (\sigma_X', \sigma_Y') \not\prec (\sigma_X, \sigma_Y)\}. \tag{S38}$$

We suppose that  $\mathcal{K}$  is a convex set in  $\mathbb{R}^2$ , which, however, has not yet been justified in terms of rigorous mathematics. Then, each point in  $\mathcal{P}$  corresponds to the minimizer of the weighted EP  $(1 - w)\sigma_X + w\sigma_Y$  for some  $w \in (0, 1)$  [11].

The minimization of  $(1 - w)\sigma_X + w\sigma_Y$  can be reduced to an optimal transport problem by squeezing the dynamics (1) as follows. We consider the squeezed coordinate  $\tilde{\mathbf{r}}$  as

$$\tilde{\mathbf{r}} = D_w \mathbf{r}, D_w := \begin{bmatrix} \sqrt{1-w} & 0 \\ 0 & \sqrt{w} \end{bmatrix}. \tag{S39}$$

The probability and mean local velocity are modified by this squeezing as  $\tilde{p}_{XY}(\tilde{\mathbf{r}}, t) = (\det D_w)^{-1} p_{XY}(D_w^{-1} \tilde{\mathbf{r}}, t)$  and  $\tilde{\mathbf{v}}(\tilde{\mathbf{r}}, t) = D_w \mathbf{v}(D_w^{-1} \tilde{\mathbf{r}}, t)$ , respectively. These satisfy the Fokker-Planck equation  $\partial_t \tilde{p}_{XY} = -\tilde{\nabla}^T (\tilde{\mathbf{v}} \tilde{p}_{XY})$ , where  $\tilde{\nabla}$  denotes the gradient



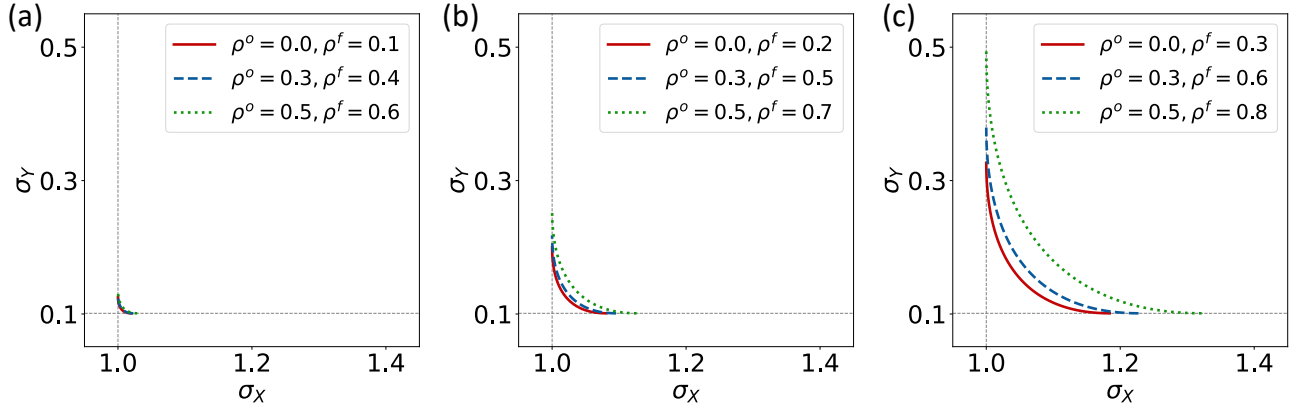


FIG. S2. The Pareto fronts of  $\sigma_X$  and  $\sigma_Y$  for the Gaussian states. These fronts are plotted for the different pairs of the correlation coefficients using Eqs. (S45)(S46): (a)  $\rho_f - \rho_o = 0.1$ , (b)  $\rho_f - \rho_o = 0.2$ , and (c)  $\rho_f - \rho_o = 0.3$ . The gray dotted lines display  $\sigma_X^*$  and  $\sigma_Y^*$  (Eq. (11)). The other parameters are  $\Sigma_{XX}^o = 1, \Sigma_{XX}^f = 4, \Sigma_{YY}^o = 3, \Sigma_{YY}^f = 2, \tau = 1$ .

in the squeezed coordinate. Since the weighted EP  $(1-w)\sigma_X + w\sigma_Y$  now has the same form as Eq. (3) in terms of  $\tilde{p}_{XY}$  and  $\tilde{v}$ , Eq. (5) can be applied to it, yielding

$$\min_{\substack{\{V,F\}_{0 \leq t \leq \tau} \\ \text{s.t. } p_{XY}^o \rightarrow p_{XY}^f}} [(1-w)\sigma_X + w\sigma_Y] = \frac{\mathcal{W}(\tilde{p}_{XY}^o, \tilde{p}_{XY}^f)^2}{\mu T \tau}. \quad (\text{S40})$$

The minimum value of the weighted EP is expressed by the Wasserstein distance between the squeezed distributions. In particular, Eq. (S40) reduces to Eq. (5) for  $w = 1/2$  (see Fig. 1).

The Pareto front of the partial EPs is obtained by plotting the minimizer of Eq. (S40) denoted as  $(\sigma_X^w, \sigma_Y^w)$  and by sweeping  $0 < w < 1$ . The minimizer and the optimal transport map  $\tilde{\mathcal{T}}^{*,w}$  in the squeezed dynamics are uniquely determined [12]. The corresponding transport map in the original dynamics is also unique and expressed as  $\mathcal{T}^{*,w}(\mathbf{r}) = D_w^{-1} \tilde{\mathcal{T}}^{*,w}(D_w \mathbf{r})$ . For  $w < w'$ ,  $\mathcal{T}^{*,w} \neq \mathcal{T}^{*,w'}$  leads to  $\sigma_X^w < \sigma_X^{w'}, \sigma_Y^w > \sigma_Y^{w'}$ , and vice versa. We note that the Pareto front collapses to a single point when  $\mathcal{T}_X^* = \mathcal{T}_{X|Y}^*$  holds (see also Fig. S2), for example,  $X$  and  $Y$  are statistically independent in both the initial and final distributions.

From another viewpoint, the minimization Eq. (S40) is considered as solving an optimal transport problem whose cost is quadratic and weighted,  $(1-w)|\mathcal{T}_X(\mathbf{r}) - x|^2 + w|\mathcal{T}_Y(\mathbf{r}) - y|^2$ . It is known that the optimal transport map of this problem converges to the Knothe-Rosenblatt map in the limit  $w \rightarrow 1$  [13, 14], which is expressed as  $\lim_{w \rightarrow 1} \mathcal{T}^{*,w} = \mathcal{T}^{*,1}$ . This also holds for the limit  $w \rightarrow 0$ . Since the optimal protocol for achieving Eq. (7) is constructed from the map  $\mathcal{T}^{*,1}$ , the endpoints of the Pareto front  $\mathcal{P}$  agree with Eqs. (7)(8):

$$\lim_{w \rightarrow 0} \sigma_X^w = \sigma_X^*, \lim_{w \rightarrow 1} \sigma_Y^w = \sigma_Y^*, \quad (\text{S41})$$

$$\lim_{w \rightarrow 1} \sigma_X^w = \sigma_X^*|_{\sigma_Y = \sigma_Y^*}, \lim_{w \rightarrow 0} \sigma_Y^w = \sigma_Y^*|_{\sigma_X = \sigma_X^*}. \quad (\text{S42})$$

## B. Gaussian Case

We exemplify the Pareto front  $\mathcal{P}$  for Gaussian distributions. In this case, the squeezed distributions are also Gaussian and given by  $p_{XY}^{o/f} = \mathcal{N}(\tilde{\mathbf{m}}^{o/f}, \tilde{\Sigma}^{o/f})$  with  $\tilde{\mathbf{m}}^{o/f} := D_w \mathbf{m}^{o/f}, \tilde{\Sigma}^{o/f} := D_w \Sigma^{o/f} D_w$ . The Wasserstein distance between these Gaussian distributions is calculated analytically as [15]

$$\mathcal{W}(\tilde{p}_{XY}^o, \tilde{p}_{XY}^f)^2 = \|\tilde{\mathbf{m}}^o - \tilde{\mathbf{m}}^f\|^2 + \text{Tr} \tilde{\Sigma}^o + \text{Tr} \tilde{\Sigma}^f - 2 \text{Tr} \left( (\tilde{\Sigma}^o)^{\frac{1}{2}} \tilde{\Sigma}^f (\tilde{\Sigma}^o)^{\frac{1}{2}} \right)^{\frac{1}{2}}, \quad (\text{S43})$$

where  $A^{1/2}$  denotes the square root of the positive definite symmetric matrix  $A$ . The optimal transport map  $\tilde{\mathcal{T}}^{*,w}$  is linear  $\tilde{\mathcal{T}}^{*,w}(\tilde{\mathbf{r}}) = G(\tilde{\Sigma}^{o-1}, \tilde{\Sigma}^f)(\tilde{\mathbf{r}} - \tilde{\mathbf{m}}^o) + \tilde{\mathbf{m}}^f$ , where  $G(A, B) := A^{\frac{1}{2}}(A^{-\frac{1}{2}}BA^{-\frac{1}{2}})^{\frac{1}{2}}A^{\frac{1}{2}}$  is the geometric mean of positive definite symmetric matrices  $A, B$  [16]. Accordingly, the corresponding transport map in the original dynamics is also linear:

$$\mathcal{T}^{*,w}(\mathbf{r}) = D_w^{-1} G(\tilde{\Sigma}^{o-1}, \tilde{\Sigma}^f) D_w (\mathbf{r} - \mathbf{m}^o) + \mathbf{m}^f =: G_w(\mathbf{r} - \mathbf{m}^o) + \mathbf{m}^f. \quad (\text{S44})$$

From Eq. (S29), the partial EPs of the corresponding protocol are calculated as

$$\sigma_X^w = \frac{1}{\mu T \tau} \left[ (m_X^o - m_X^f)^2 + \Sigma_{XX}^o + \Sigma_{XX}^f - 2 \text{Tr} (D_0 G_w \Sigma^o) \right], \quad (\text{S45})$$

$$\sigma_Y^w = \frac{1}{\mu T \tau} \left[ (m_Y^o - m_Y^f)^2 + \Sigma_{YY}^o + \Sigma_{YY}^f - 2 \text{Tr} (D_1 G_w \Sigma^o) \right]. \quad (\text{S46})$$

The blue curve in Fig. 3(d) is obtained by plotting these EPs for  $0 < w < 1$ . The Pareto front contracts to a single point if and only if  $\rho_o = \rho_f$  (see Eqs. (12)(S18)). The Pareto front expands further as  $|\rho_o - \rho_f|$  increases (see Fig. S2).

We examine the limits of  $w \rightarrow 0$  and  $w \rightarrow 1$  to validate Eqs. (S41)(S42). Using the relation  $\text{Tr} A^{\frac{1}{2}} = \sqrt{\text{Tr} A + 2 \det A^{\frac{1}{2}}}$  for the positive definite symmetric matrix  $A$  of size 2, it can be shown that the limits of these EPs satisfy Eq. (S41), where  $\sigma_X^*, \sigma_Y^*$  are given by Eq. (11). Furthermore, one can confirm that the limit of  $G_w$  agrees with (S19), that is,  $\lim_{w \rightarrow 1} G_w = G_1$  from the asymptotic analysis. This also holds for the limit  $w \rightarrow 0$ . Thus, Eq. (S42) is verified through the calculation of Eqs. (S45)(S46), where  $\sigma_X^*|_{\sigma_Y=\sigma_Y^*}, \sigma_Y^*|_{\sigma_X=\sigma_X^*}$  are given by Eq. (11).

- 
- [S1] U. Seifert, Stochastic thermodynamics, fluctuation theorems and molecular machines, Rep. Prog. Phys. **75**, 126001 (2012).
  - [S2] T. M. Cover, *Elements of information theory* (John Wiley & Sons, 1999).
  - [S3] A. E. Allahverdyan, D. Janzing, and G. Mahler, Thermodynamic efficiency of information and heat flow, Journal of Statistical Mechanics: Theory and Experiment **2009**, P09011 (2009).
  - [S4] J. M. Horowitz and M. Esposito, Thermodynamics with continuous information flow, Phys. Rev. X **4**, 031015 (2014).
  - [S5] C. Villani, *Topics in Optimal Transportation*, 58 (American Mathematical Soc., 2003).
  - [S6] M. Nakazato and S. Ito, Geometrical aspects of entropy production in stochastic thermodynamics based on Wasserstein distance, Phys. Rev. Res. **3**, 043093 (2021).
  - [S7] C. Villani, *Optimal transport: old and new*, Vol. 338 (Springer, 2009).
  - [S8] T. Kamijima, K. Funo, and T. Sagawa, Finite-time thermodynamic bounds and tradeoff relations for information processing, arXiv preprint arXiv:2409.08606 (2024).
  - [S9] P. Ngatchou, A. Zarei, and A. El-Sharkawi, Pareto multi objective optimization, in *Proceedings of the 13th International Conference on, Intelligent Systems Application to Power Systems* (IEEE, 2005) pp. 84–91.
  - [S10] C. Coello, *Evolutionary Algorithms for solving Multi-Objective Problems* (Springer, 2007).
  - [S11] R. T. Marler and J. S. Arora, The weighted sum method for multi-objective optimization: new insights, Structural and multidisciplinary optimization **41**, 853 (2010).
  - [S12] W. Gangbo and R. J. McCann, The geometry of optimal transportation, Acta Mathematica **177**, 113 (1996).
  - [S13] G. Carlier, A. Galichon, and F. Santambrogio, From Knothe’s transport to Brenier’s map and a continuation method for optimal transport, SIAM Journal on Mathematical Analysis **41**, 2554 (2010).
  - [S14] F. Santambrogio, Optimal transport for applied mathematicians, Birkäuser, NY **55**, 94 (2015).
  - [S15] C. R. Givens and R. M. Shortt, A class of Wasserstein metrics for probability distributions., Michigan Mathematical Journal **31**, 231 (1984).
  - [S16] R. Bhatia, T. Jain, and Y. Lim, On the Bures–Wasserstein distance between positive definite matrices, Expositiones Mathematicae **37**, 165 (2019).